A Dictionary Learning Approach for Joint Reconstruction and Denoising in Low Field Magnetic Resonance Imaging

Ahishakiye, Emmanuel ; van Gijzen, Martin Bastiaan; Shan, Xiujie; Tumwiine, Julius ; Obungoloch, Johnes

Publication date
2021

Document Version
Final published version

Published in
2021 IST-Africa Conference (IST-Africa)

IST-Africa

IST-Africa 2021 Conference Proceedings
Miriam Cunningham and Paul Cunningham (Eds)
IST-Africa Institute and IIMC, 2021
ISBN: 978-1-905824-67-0

A Dictionary Learning Approach for Joint Reconstruction and Denoising in Low Field Magnetic Resonance Imaging

Emmanuel AHISHAKIYE[1,2], Martin Bastiaan VAN GIJZEN[3], Xiujie SHAN[4], Julius TUMWIINE[5], Johnes OBUNGOLOCH[2]

[1]*Department of Computer Science, Kyambogo University, PO Box 1, Kampala, Uganda*
[2]*Department of Biomedical Sciences and Engineering, Mbarara University of Science and Technology, Mbarara, 1410, Uganda, Tel: +256787371879, +256775646496*
Email: ahishema@gmail.com, jobungoloch@must.ac.ug
[3,4]*Delft Institute of Applied Mathematics, Delft University of Technology, The Netherlands, Email: M.B.vanGijzen@tudelft.nl*
[4]*Harbin Institute of Technology, 92 Xidazhi St, Nangang, Harbin, Heilongjiang, China*
[5]*Department of Mathematics, Mbarara University of Science and Technology, P.O. Box 1410, Mbarara, Uganda, Email: jtumwiine@must.ac.ug*

Abstract: Currently, many children with hydrocephalus in East Africa and other resource-constrained countries do not have access to Magnetic Resonance Imaging (MRI) scanners, the preferred imaging tool during the disease administration and treatment. Conventional MRI scanners are costly to buy and manage, which limits their utilization in low-income countries. Low-field MRI scanners can offer an affordable, sustainable, and safe imaging alternative to high-field MRI. However, they are associated with a low signal-to-noise ratio (SNR), and therefore the images obtained are noisy. In this study, we propose an algorithm that may help to alleviate the drawbacks of low-field MRI by improving the quality of images obtained. The proposed algorithm combines our previous proposed algorithm known as AS-DLMRI for image reconstruction and a nonlinear diffusion filter for image denoising. The formulation is capable of removing additive zero-mean white and homogeneous Gaussian noise, as well as other noise types that could be present in the original signal. Experiments on visual quality revealed that the proposed algorithm is effective in denoising images during reconstruction. The proposed algorithm effectively denoised a noisy phantom, and a noisy MRI image, and had better performance when compared to DLMRI and AS-DLMRI in terms of Peak Signal to Noise ratio (PSNR) and High-Frequency Error Norm (HFEN). Integrating AS-DLMRI and the nonlinear diffusion filter proved to be effective in improving the quality of the images during the experiments performed. The hybrid algorithm may be of great use in imaging modalities like low-field MRI that are associated with low SNR.

Keywords: MRI, low-field MRI, image reconstruction, Dictionary learning, Image denoising.

1. Introduction

Hydrocephalus is the build-up of cerebrospinal fluid in the cavities within the brain. It can be fatal if left untreated. There are an estimated 200,000 new cases of hydrocephalus every year in sub-Saharan Africa alone [1]. Magnetic Resonance Imaging (MRI) is a widely used imaging modality for intracranial diseases. Currently, many children with hydrocephalus in East Africa and other resource-constrained countries do not have access to conventional

MRI scanners, the preferred imaging tool during the disease administration and treatment. Conventional MRI scanners are expensive to buy and manage, which limits their utilization in low-income countries. Low-field MRI systems can offer an affordable, sustainable, and safe imaging alternative to high-field MRI and computed tomography (CT) for brain imaging of hydrocephalus in developing countries [2]. Mbarara University of Science and Technology (MUST) in Uganda has an ongoing collaboration with Leiden University Medical Center (LUMC) in the Netherlands, Pennsylvania State University (PSU) in the USA and the Delft University of Technology (TU Delft) in the Netherlands to develop a low-field MRI system for hydrocephalus diagnosis in Uganda. Figure 1 shows the low-field MRI systems under development, for details refer to [3], [2], [4], [5]. The low-field MRI scanners under development are characterized by a low signal-to-noise ratio (SNR) which results in noisy images. During our previous study, we proposed an algorithm for image reconstruction, called AS-DLMRI [6], which was developed to address this challenge. Experimental results revealed that AS-DLMRI was not effective when the input signal was too noisy. In this study, we extend our previous work by proposing a joint image reconstruction and denoising algorithm by combining the AS-DLMRI algorithm with a nonlinear diffusion filter. We anticipate that the proposed algorithm may result in sufficiently high-quality images that are required for hydrocephalus treatment planning, as well as accelerating the acquisition speed.

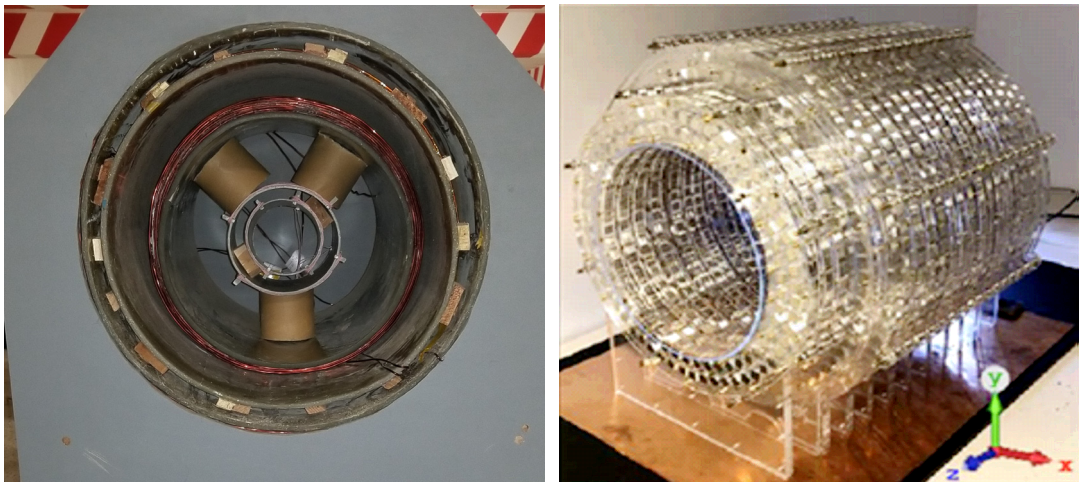

Figure 1: The low-field MRI prototypes. The left is the PSU-MUST prototype, adapted from [3]; and the right is the LUMC prototype, adapted from [4].

1.1 Research objectives and Outline

This study is part of the project funded by the Dutch organization NWO-WOTRO working towards developing low-cost MRI scanners to aid in the treatment of hydrocephalus at CURE children's hospital in Uganda. By developing low-cost MRI scanners, the study contributes to Sustainable Development Goals (SDG) 3, "Ensure healthy lives and promote well-being for all at all ages". These low-field MRI scanners under development yield noisy images [7] that requires enhancement before being used by clinicians in their diagnosis tasks, and other subsequent operations like segmentation. We aim to combine our earlier algorithm, AS-DLMRI [6] with the nonlinear diffusion filtering technique described in section 2.2. The result of this combination is a hybrid algorithm capable of simultaneous reconstruction and denoising during the program's execution. Adopting an integrated acquisition-reconstruction-denoising process may provide a more efficient and accurate solution, and therefore worth exploring [8]. The major objective of this study is to develop and implement a joint image reconstruction-denoising algorithm suitable for medical imaging devices as low-field MRI systems that are characterized by noise. We aim to

alleviate the drawbacks of the low-field MRI with the algorithm proposed and described in this paper.

The rest of the paper is organized as follows. In section 2, the methodology is discussed; section 2.1 discusses the adaptive-size image reconstruction in MRI; section 2.2 discusses image denoising using a nonlinear diffusion filter, and section 2.3 discusses the summary of our proposed algorithm. In section 3, experimental results are discussed. In section 4, we discuss the results, conclusions and outlook are given in section 5.

2. Materials and Methods

2.1 Adaptive-size Image reconstruction

The dictionary learning procedure for image reconstruction aims to solve the optimization problem presented in equation (1). The formulation F0 was obtained from Ravishankar and Bresler [9].

$$(F0)\ \min_{x,D,\Gamma} \sum_{ij} \left\| R_{ij}x - D\alpha_{ij} \right\|_2^2 + w \left\| F_u x - y \right\|_2^2 \quad \text{subject to } \left\| \alpha_{ij} \right\|_0 \leq T_0 \forall_{i,j}, \quad (1)$$

where the first part of the formulation in equation (1) captures the quality of sparse approximations of the image patches in relation to the dictionary D, the second part enforces data fidelity in the k-space, Γ denotes the set $\{\alpha_{ij}\}_{ij}$ of sparse representations of all patches, the matrix $R_{ij}x \in C^{n\times q}$ extracts the patch $x_{i,j}$ from x as $x_{i,j} = R_{ij}x$, T_0 represents the sparsity level, F_u is the undersampled Fourier transform and the ℓ_0 quasi norm encodes the sparsity of the patch representation. The weight w is defined as $w = (\lambda/\delta)$, where δ is the standard deviation λ is a positive constant. The image reconstruction formulation in equation (1) is nonconvex and non-deterministic polynomial-time hard (NP-hard) even when the ℓ_0 norm is relaxed to ℓ_1 norm [9]. To address this challenge, a two-step alternating minimization procedure is described below.

The dictionary learning step acts as the first step, and it involves fixing x and then learning the dictionary D and sparse representations of the patches jointly. The initial size of the dictionary is n_{init} and the dictionary is initialized with the left singular vectors of the training data. The Approximate K-SVD (AK-SVD) algorithm [10] and OMP [11] is used to learn the dictionary, and for sparse coding, respectively. Information-Theoretic Criteria (ITC) are used in this step to sort the candidate dictionaries to establish the optimal size. The ITC used is called Extended Bayesian Information Criterion (EBIC) [12]. For a given training signal $Y \in C^{mxN}$, the EBIC is computed as $EBIC = 2log\ RMSE + \frac{log(Q)}{(Q)}P + \frac{2N}{(Q)}log\binom{n}{s}$, where $RMSE$ is the root mean square error, P is complexity, and $Q = mN$, m and N are the dimensions of the training signal. A small number of candidates n_{cand} is considered to avoid over computation. During selection, dictionaries $D_h \in C^{mxh}$ are considered, where $h \leq n$ atoms of D, and there are at most n candidate dictionaries. A lower bound $n_{\min}$ helps to eliminate small dictionaries that are not useful. During this study, $n \geq n_{\min}$ and $n_{min} = m$ are chosen. Also, n_{ITC} is the minimum size of the ITC value among n_{cand}. The dictionary size n is adjusted based on the following conditions (i) if n_{ITC} is smaller than the current dictionary size n, n is then decreased by e-, (ii) if n_{ITC} is slightly smaller than the current dictionary size n, n is then decreased by 1, and (iii) if n_{ITC} is equal to n, n is then increased by e+. In this study, a 5 was used for e- and e+. After P iterations, the value n_{ITC} is considered as the true dictionary size. For more details, refer to [6] [12].

The first step is then followed by the second step in which the dictionary and the sparse representations are fixed and x is updated. This is achieved by solving a least-squares problem in equation (2) below.

$$Fx(k_x,k_y) = \begin{cases} M(k_x,k_y), & (k_x,k_y) \notin \Omega \\ \frac{M(k_x,k_y)+w\,M_o(k_x,k_y)}{1+w}, & (k_x,k_y) \in \Omega, \end{cases} \quad (2)$$

where $Fx(k_x,k_y)$ is the updated value at a location (k_x,k_y), $M_0 = FF_u^H y$ are the zero-filled k-space measurements, and Ω is the subset of k-space that has been sampled. Then the reconstructed image x is obtained by IFFT of Fx. For more details, refer to [9].

2.2 Image denoising using a nonlinear diffusion filter

In this step, image denoising is done using a nonlinear diffusion filter. Using a nonlinear diffusion filtering technique, the pixel intensities are interpreted as a physical quantity that spreads by a diffusion process in the image. The simplest diffusion-filtering model for image denoising is the standard heat diffusion. Below is a description of the first nonlinear model that was proposed by Perona and Malik [13].

$$\begin{aligned} &\frac{\partial u}{\partial t} = \nabla . (c(\| \nabla u \|)\nabla u) \text{ in } \Omega\, x\, (0,T), \\ &u(x,0) = f \text{ in } \Omega, \\ &\frac{\partial u}{\partial n} = 0 \text{ on } \partial\Omega\, x\, (0,T), \end{aligned} \quad (3)$$

where Ω is the image domain, T is the stopping time, u is the complex pixel value, f is the noisy image, and c is a nonnegative monotonically decreasing function with $c(0) = 1$ and $c(+\infty) \to 0$. In this work, we use the function

$$\left(c(\| \nabla u \|)\right) = e^{-\left(\frac{\|\nabla u\|}{K}\right)^2} \quad (4)$$

This function was originally proposed in [13]. The damping parameter K can be used to influence how sensitive the function c is with respect to the value of the norm of the gradient. In our experiments we use K=10. To discretize equation (3) in space, the standard finite difference is used, see [13] for the details. Explicit Euler is used to discretize in time. The images are denoised using 10-time steps. In this paper, we use a simple explicit method. We refer to [14] for more advanced implicit methods for denoising.

2.3 Summary of the proposed algorithm

Our proposed algorithm incorporates image reconstruction and denoising as explained in subsections (2.1) and (2.2), respectively. The summary of the proposed algorithm is shown in Figure 2 below.

Algorithm 1: Proposed algorithm for medical Image reconstruction and denoising

---

Input: $k-space\ measurements$, *s, initial* D_{size}, n_{cand}, *e+, e-, P (maximum number of iterations) and c (the number of iterations between dictionary size changes)*
Output: *x- Reconstructed noise-free image*

Initialization: set $n \leftarrow n_{init}$, also, initialize the dictionary with zero-filled Fourier reconstruction.
for p = 1 : P **do**
  Dictionary Learning step: learn **D** with AK-SVD [10] and sparse representations with OMP [11].
  if p mod c = 0 **then**
    Sort atoms of the dictionary **D**
    Compute ITC values for dictionaries **D** (:, 1 : *h*), with *h*= n- n_{cand} + 1 : n
    Let n_{ITC} be the size for which ITC is minimum
    if n_{ITC} = n **then**
      Increase the size: n ← n + e+
    else
      if n_{ITC}< n **then**
        Decrease the size by e-: n ← n – *e-*
      else
        decrease the size by 1: n ← n – 1
      Trim dictionary: **D** (:, 1: n)
  Set n ← n_{ITC}, and run k more iterations for final refinement

17 Update x: each pixel value obtained by averaging contributions of patches that cover it
18 M ← FFT(x)
19 Restore sampled frequencies to update M using equation (2).
20 x ← IFFT(M)
21 Denoise x using a diffusion filter described in subsection 2.2
22 **end for**

Figure 2. The proposed hybrid algorithm

3. Experimental Results

This section explains the performance parameters used during this study. We evaluate our method on three images: a phantom image obtained from [4], an MRI brain image obtained from [9], and a hydrocephalic image obtained from [15], as shown in Figure 3. PSNR, HFEN, and reconstruction time (in seconds) were also used as performance parameters in this study. The proposed algorithm was initialized with a zero-filled Fourier reconstruction. All the images used were converted into overlapping patches of size $\sqrt{n} \times \sqrt{n}$, $n = 36$. The dictionary was initialized with the left singular vectors of the training data. Also, sparsity level, s=5, $n_{\min} = 64$, $n_{minus} = 5$, $n_{plus} = 5$, $n_{cand} = 20$, $ITC_{index} = 11$, $K = n = 36$, sparsity τ_0 = 6, $\gamma = 140$, overlap stride $r = 1$. For denoising, the time step=1e-05, and the number of time steps = 10. The proposed algorithm was also compared with two other dictionary learning-based image reconstruction algorithms, these are; DLMRI [9] and AS-DLMRI [6]. The Matlab implementation of DLMRI is available from authors' websites, and the built-in settings were used in all the experiments. We are extending AS-DLMRI, our previous study, and we also maintained its previous settings. The undersampling masks used with several downsampling factors were obtained from [9]. All the experiments were done using Matlab 2017a.

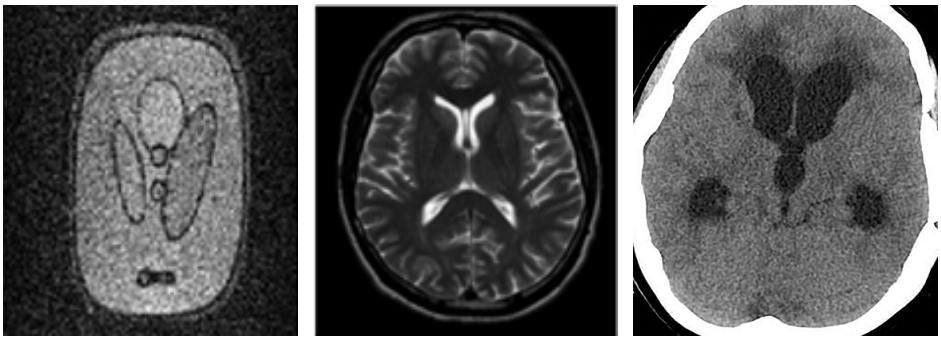

Figure 3. (Left) The 2D phantom, (Middle) an MRI Brain Image, and (Right) Hydrocephalic image.

3.1 Experiments on Reconstruction Visual Quality

This experiment was done to determine the visual quality of the reconstructed images using the proposed algorithm, DLMRI, and AS-DLMRI. For the results shown in Figure 4 below, a sampling mask in k-space with 20-fold undersampling, and the number of iterations was fixed at 20 were used. During this experiment, we used the Phantom image obtained from [4], the MR image from [9], we also corrupted this MR image by 20dB of noise to obtain another noisy image, and a hydrocephalus image obtained from [15]. It was noted that the visual quality for the images reconstructed by the proposed algorithm was better than those with ASDLMRI and DLMRI. Other experiments were done with different undersampling masks (2.5, 4, 6, 10) and altering the number of iterations for dictionary learning. It was observed that the proposed algorithm consistently removed noise artifacts from the reconstructed images. Figure 4 shows the reconstructed images.

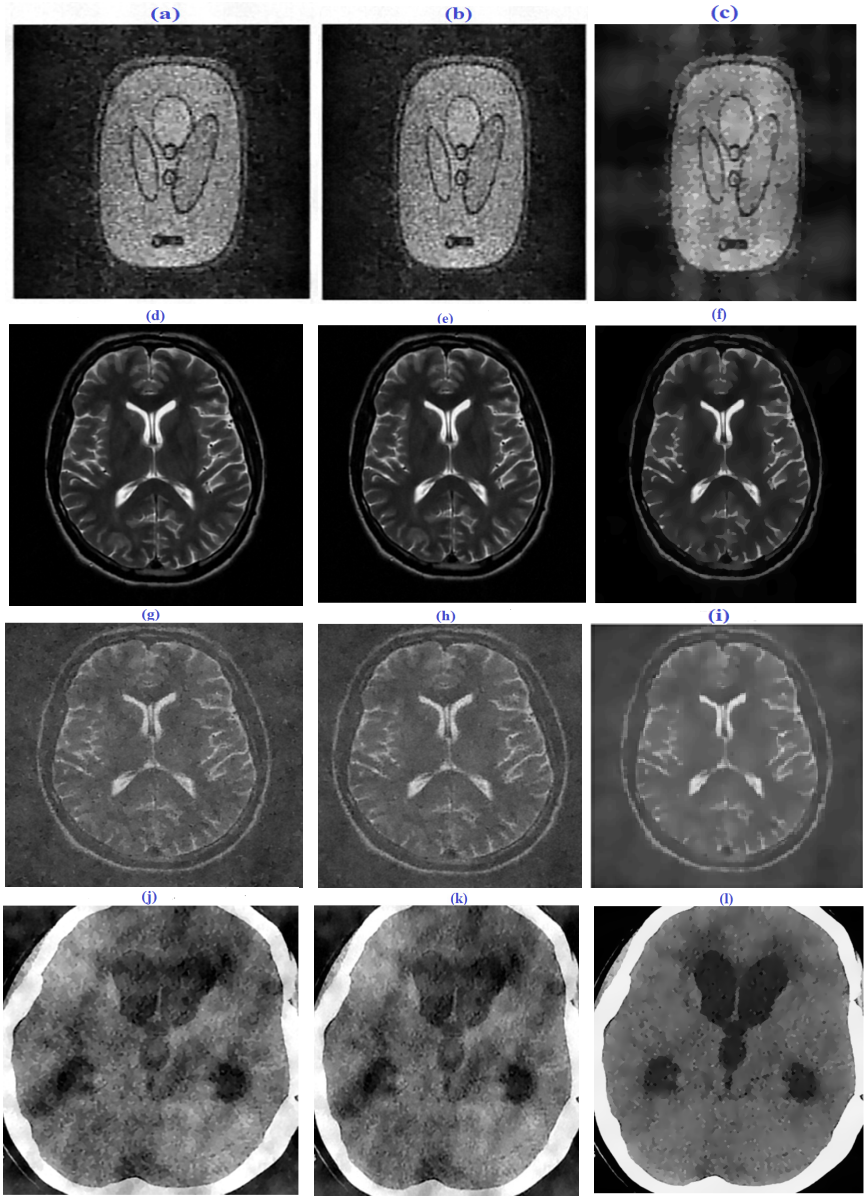

Figure 4: Reconstructed Images. (a) Phantom image reconstructed by DLMRI, (b) reconstruction by AS-DLMRI, and (c) reconstruction by the proposed algorithm. in (d), reconstruction of MRI image using DLMRI, (e) by AS-DLMRI, and (f) by our proposed algorithm. in (g), reconstruction of a noisy MRI image using DLMRI, (h) by AS-DLMRI, and (i) by our proposed algorithm. In (j), reconstruction of a hydrocephalus image by DLMRI, (k) using AS-DLMRI, and (l) using our proposed algorithm.

3.2 Performance of the algorithms on PSNR, HFEN, and iteration number

During this experiment, we used the images described in section 3. Experimental results revealed that our proposed algorithm produced higher PSNR compared to DLMRI and AS-DLMRI as shown in figure 5. The values of PSNR increased as the number of iterations increases in all the algorithms. Higher values of PSNR reveal that our proposed algorithm reconstructs better quality images when compared to DLMRI and AS-DLMRI. More so, it was observed that our proposed algorithm resulted in low values of HFEN when compared to DLMRI and AS-DLMRI. Also, the values of HFEN continued to decrease as the number of iterations increased indicating the superior performance of the proposed algorithm in capturing edges and fine features of the reconstructed images.

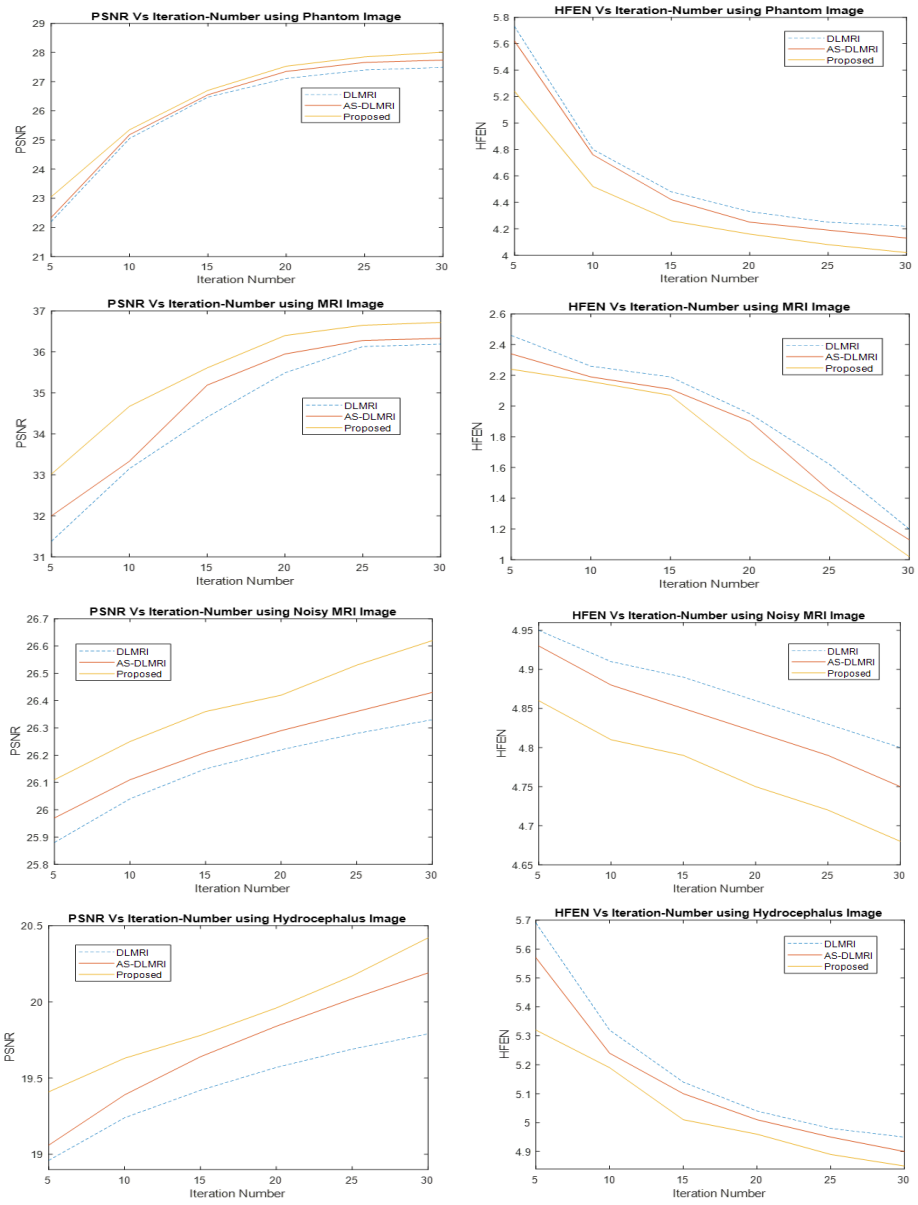

Figure 5: Experiments on PSNR, HFEN, and Iteration Number. The top row shows experiments using a phantom image, the second row from the top shows experiments using MRI image, the second last row shows experiments with a noisy MRI image and finally, the last row shows experiments with a hydrocephalus image.

3.3 Experiment on PSNR, HFEN and Undersampling Mask

This experiment was done to understand how various undersampling masks affect the PSNR and hence the quality of the reconstructed images. We also used all images described in section 3.1. we used undersampling masks of 2.5, 4, 6, 8, 10, and 20. During this experiment, it was revealed that the values of PSNR decreased with an increase in the size of the undersampling mask with all the algorithms. However, our proposed algorithm had better PSNR when compared to DLMRI and AS-DLMRI. Experiments on HFEN revealed that the values increase as the size of the undersampling mask increases. Our proposed algorithm resulted in lower values of HFEN when compared to DLMRI and HFEN. Figure 6 shows the results of the experiment.

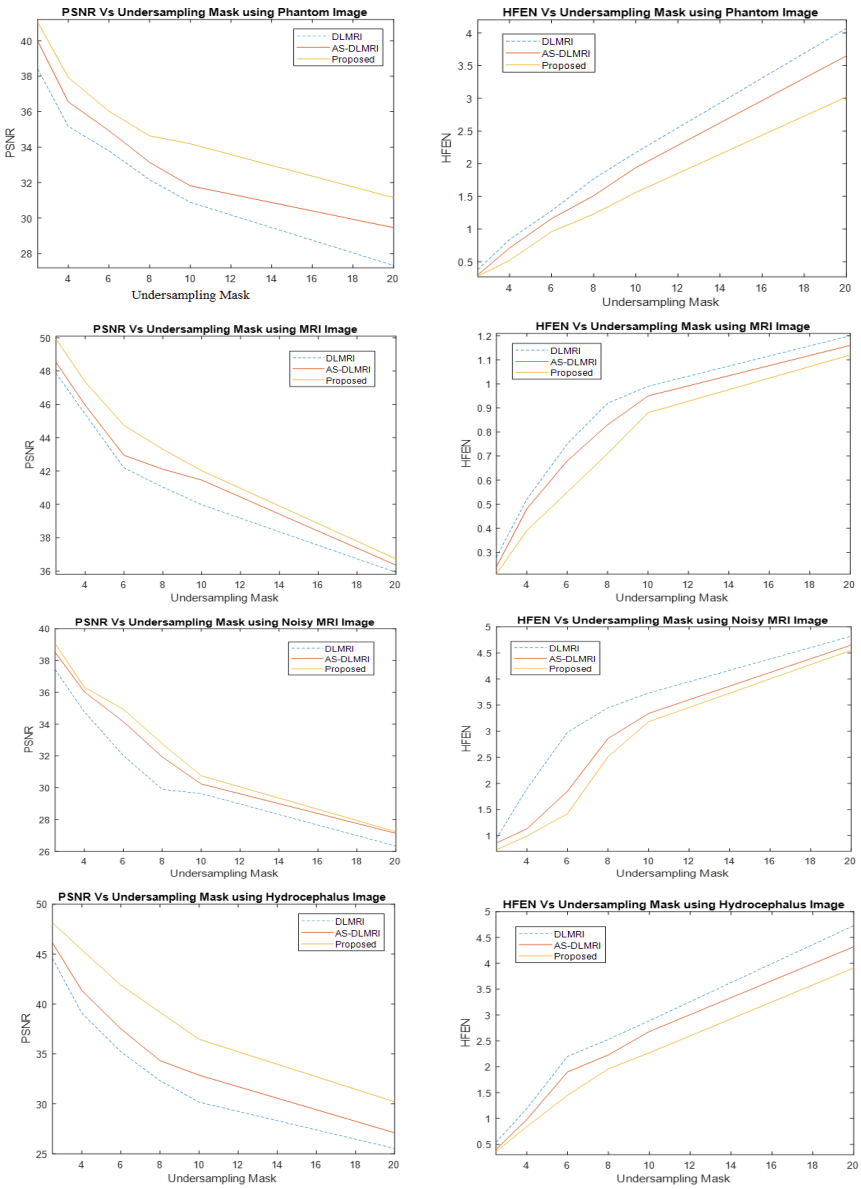

Figure 6: Experiments on PSNR, HFEN, and Undersampling Mask. The top row shows experiments using a phantom image, the second row from the top shows experiments using MRI image, the second last row shows experiments with a noisy MRI image and finally, the last row shows experiments with a hydrocephalus image.

4. Discussion

This study discusses an algorithm that integrates adaptive-size dictionary learning and diffusion filtering for joint image reconstruction and denoising in low field MRI. The performance of the proposed algorithm was compared to existing state-of-art methods. The phantom image, MRI image, and hydrocephalus image were used in all the experiments. The PSNR and HFEN were used as the performance metrics during the evaluation of the algorithm. These metrics were selected because they have been used in related studies. We evaluated the performance of our proposed algorithm in comparison with DLMRI and AS-DLMRI. Also, all the experiments were done on a computer with a standard central processing unit (CPU) and no graphical processing unit (GPU). Experiments on visual quality revealed that the proposed algorithm is effective in denoising an image during reconstruction. The proposed algorithm effectively denoised a noisy phantom, and a noisy MRI image, and had better performance when compared to DLMRI and AS-DLMRI in terms of PSNR and HFEN. Our proposed algorithm also exhibited superior performance

with various undersampling factors as shown by the experimental results above. The proposed algorithm also requires low computing power since it does not require special computing devices like GPU. The proposed algorithm may be suitable for use in resource-constrained environments like Uganda where access to high-end computing resources GPUs is still limited.

5. Conclusions and Outlook

In the study, an algorithm for joint image reconstruction and denoising in medical imaging was implemented. The image reconstruction part was done using adaptive dictionary learning with Information-Theoretic Criteria (ITC), while the denoising part was done using a diffusion filter. The performance of the proposed algorithm with two leading dictionary learning-based algorithms, that is, DLMRI and AS-DLMRI was done. Experimental results revealed that the proposed algorithm is effective in producing noise-free reconstructions especially when the input signal is noisy. Also, the proposed algorithm is effective in removing noise from the reconstructed images. Experiments on PSNR and HFEN revealed the better performance of our proposed algorithm when compared to DLMRI and AS-DLMRI. Combining image reconstruction and denoising could save time and other image details that could be lost due to having two separate operations in medical image processing. The proposed algorithm may be used in imaging modalities like low-field MRI where the image signal is noisy. Experimental results revealed that integrating AS-DLMRI and diffusion filter may be effective in improving the quality of the images in low-field MRI. The next step of our research is to add a segmentation function to the proposed algorithm since it is a necessary step required for the diagnosis of hydrocephalus.

Acknowledgment

This research was made possible through the Dutch organization NWO-WOTRO grant nr. W 07.303.101: 'A sustainable MRI system to diagnose hydrocephalus in Uganda'. The authors gratefully acknowledge NWO for their financial support. The authors thank Tom O. Reilly for making available to us the image phantoms from the low-field MRI scanners. We also thank S. Ravishankar and Y. Bresler, B. Dumitrescu, and C. D. Giurc˘aneanu for making their research codes available.

References

[1] K. T. Kahle, A. V. Kulkarni, D. D. Limbrick, and B. C. Warf, "Hydrocephalus in children," *Lancet*, vol. 387, no. 10020, pp. 788–799, 2016, doi: 10.1016/S0140-6736(15)60694-8.

[2] J. Obungoloch *et al.*, "Design of a sustainable prepolarizing magnetic resonance imaging system for infant hydrocephalus," *Magn. Reson. Mater. Physics, Biol. Med.*, pp. 1–21, 2018, doi: 10.1007/s10334-018-0683-y.

[3] M. de L. den Bouter *et al.*, "Description of a Low-field MRI Scanner Based on Permanent Magnets," in *CEUR Workshop Proceedings (CEUR-WS.org)*, 2020, pp. 1–15.

[4] T. O. Reilly and A. Webb, "Deconstructing and reconstructing MRI hardware," *J. Magn. Reson.*, vol. 306, pp. 134–138, 2019, doi: 10.1016/j.jmr.2019.07.014.

[5] T. O'Reilly, W. M. Teeuwisse, and A. G. Webb, "Three-dimensional MRI in a homogenous 27 cm diameter bore Halbach array magnet," *J. Magn. Reson.*, vol. 307, p. 106578, 2019, doi: 10.1016/j.jmr.2019.106578.

[6] E. Ahishakiye, M. B. Van Gijzen, J. Tumwiine, and J. Obungoloch, "Adaptive-size dictionary learning using information-theoretic criteria for image reconstruction from undersampled k-space data in low field magnetic resonance imaging," *BMC Med. Imaging*, pp. 1–12, 2020, doi: 10.1186/s12880-020-00474-3.

[7] M. L. de Leeuw den Bouter, M. B. van Gijzen, and R. F. Remis, "Conjugate gradient variants for L_p regularized image reconstruction in low□field MRI," *SN Appl. Sci.*, vol. 1, no. 12, pp. 1–15, 2019, doi: 10.1007/s42452-019-1670-2.

[8] E. Ahishakiye, M. B. Gijzen, J. Tumwiine, and J. Obungoloch, "A Dictionary Learning Approach for Noise-Robust Image Reconstruction in Low-Field Magnetic Resonance Imaging," in *IST-Africa 2020 Conference Proceedings, Paul Cunningham and Miriam Cunningham (Eds), IST-Africa Institute and*

IIMC, 2020, ISBN: 978-1-905824-64-9.
[9] S. Ravishankar and Y. Bresler, “MR Image Reconstruction From Highly Undersampled k-Space Data by Dictionary Learning,” *IEEE Trans. Med. Imaging*, vol. 30, no. 5, pp. 1028–1041, 2011, doi: 10.1109/TMI.2010.2090538.
[10] R. Rubinstein, M. Zibulevsky, and M. Elad, “Efficient Implementation of the K-SVD Algorithm using Batch Orthogonal Matching Pursuit,” *Comput. Sci. Dep. - Teh. Rep. CS-2008-08.revised - 2008*, no. January 2008.
[11] Y. C. Pati, R. Rezaiifar, and P. S. Krishnaprasad, “Orthogonal matching pursuit: recursive function approximation with applications to wavelet decomposition,” in *Conference Record of the Asilomar Conference on Signals, Systems & Computers*, 1993, vol. 1, pp. 40–44, doi: 10.1109/acssc.1993.342465.
[12] B. Dumitrescu and C. D. Giurc˘aneanu, “Adaptive-Size Dictionary Learning Using Information Theoretic Criteria,” *MDPI-Algorithms*, pp. 1–13, 2019, doi: 10.3390/a12090178.
[13] P. Perona and J. Malik, “Scale-Space and Edge Detection Using Anisotropic Diffusion,” *IEEE Trans. Pattern Anal. Mach. Intell.*, vol. 12, no. 7, 1990.
[14] X. Shan and M. van Gijzen, "Deflated Preconditioned Conjugate Gradients for Nonlinear Diffusion Image Enhancement," Numerical Mathematics and Advanced Applications ENUMATH 2019, F.J. Vermolen and C Vuik Eds. Lecture Notes in Computational Science and Engineering, 139, 2021.
[15] W. N. Gibbs and L. N. Tanenbaum, “Imaging of hydrocephalus,” *Appl. Radiol.*, vol. 47, no. 5, pp. 5–13, 2018.